Visualization of the Internal Cerebral Veins on MR Phase-Sensitive Imaging: Comparison with 3D Gadolinium-Enhanced MR Venography and Fast-Spoiled Gradient Recalled Imaging

TECHNICAL NOTE

J. Sun
J. Wang
L. Jie
H. Wang
X. Gong

SUMMARY: The purpose of this article is to compare the visualization quality of ICV and their tributaries on PSI-MRV, 3D CE-MRV, and 3D CE-FSPGR. PSI-MRV has been shown to delineate the ICV, TSV, SV, anterior caudate nucleus veins, and medial atrial veins effectively. Due to its advantages of no contrast material injection, acceptable examination times, and no arterial contamination, PSI-MRV should be considered in the evaluation of deep cerebral veins.

ABBREVIATIONS: 3D CE-FSPGR = 3D contrast-enhanced fast-spoiled gradient recalled imaging; 3D CE-MRV = 3D contrast-enhanced MR venography; ICV = internal cerebral veins; MinIP = minimum intensity projection; MIP = maximum intensity projection; MRV = MR venography; PSI = phase-sensitive imaging; PSI-MRV = phase-sensitive imaging-based MR venography; SV = septal veins; SWI = susceptibility-weighted imaging; TSV = thalamostriate veins

Deep cerebral veins have received increasing attention due to their importance in preoperational planning.[1,2] Various MRV technologies have been developed for imaging the deep cerebral veins, including the ICV, noninvasively. However, displaying the ICV and their tributaries is still a challenge for noncontrast or contrast MRV, though the image quality has improved with the advent of higher field systems.[3,4] SWI uses the paramagnetic deoxygenated hemoglobin in veins, which causes a shift in resonance frequency between the venous vessel and surrounding tissue, as an intrinsic contrast agent. In SWI-based venography, high spatial resolution increases the venous blood volume fraction within a voxel and leads to a better visualization of small venous structures.[5,6] SWI is called PSI, as implemented on the Signa Excite HD scanner (GE Healthcare, Milwaukee, Wisconsin).[7] The purpose of this study was to evaluate the applicability of PSI-MRV in detecting the ICV and their tributaries through a comparison with 3D CE-MRV and 3D CE-FSPGR.

Technique

Patients

After obtaining the approval of the hospital ethics committee and written informed consent of patients, 65 consecutive patients with supratentorial meningioma were examined with 3D CE-MRV for presurgical evaluation of intracranial dural sinuses. PSI-MRV and 3D CE-FSPGR were performed before and after 3D CE-MRV.

Twelve patients were excluded because the meningioma caused severe distortion of the third or lateral ventricular area. Nine patients were excluded because motion artifacts occurred in at least 1 of the 3 MRV examinations. Four patients who underwent repeat surgery were excluded because their images could not be evaluated due to susceptibility artifacts caused by hemorrhage around the ventricular area. A total of 40 patients (21 women and 19 men; age range, 22-77 years; mean age, 53.9 years) were enrolled.

Imaging Examinations

All MR imaging studies were performed on a 3T system (Signa Excite HD, GE Healthcare) equipped with an 8-channel phased array head coil. The MR imaging scanning field covered the bilateral hemispheres, including the ICV and their main tributaries. After conventional T1-weighted and T2-weighted imaging, PSI-MRV, 3D CE-MRV, and 3D CE-FSPGR were performed in order. 3D CE-MRV consisted of 2 scans with an acquisition time of 59 seconds each. A dose of 0.05-mmoL/kg gadolinium contrast material was administered intravenously with an injector at a rate of 3 mL/s immediately after the first scan. A repeat scan with the same parameters was obtained after a 20-second delay. 3D CE-FSPGR was performed after the 3D CE-MRV sequence. The imaging parameters are listed in Table 1.

Image Reconstruction

The MR images were postprocessed with an Advantage Workstation version 4.2 (GE Healthcare). For PSI-MRV, images were reformatted

Table 1: Imaging parameters in PSI, 3D CE-MRV, and 3D CE-FSPGR sequences

Parameter	PSI	3D CE-MRV	3D CE-FSPGR
Orientation	Axial	Sagittal	Axial
TR (ms)	40	3.1	7.8
TE (ms)	26	0.9	3.8
Flip angle	20°	25°	25°
Slab thickness (mm)	80	160	160–180
Section thickness (mm)	2	1	0.7
FOV (mm)	240	260	240
Pixel matrix	320 × 288	288 × 256	320 × 256
NEX	0.75	1	2
Acquisition time (min/sec)	4.57	1.50	5.47–7.43

Table 2: A comparison of the visualization of ICV and tributaries on the 3 different MRV techniques

	MRV						PSI-MRV/	PSI-MRV/	3D CE-MRV/
	PSI-MRV		3D CE-MRV		3D CE-FSPGR		3D CE-MRV	3D CE-FSPGR	3D CE-FSPGR
Veins	Range	Mean	Range	Mean	Range	Mean			
ICV	3–3	3.00 ± 0.00	3–3	3.00 ± 0.00	3–3	3.00 ± 0.00	None	None	None
TSV	3–3	3.00 ± 0.00	3–3	3.00 ± 0.00	3–3	3.00 ± 0.00	None	None	None
SV	2–3	2.90 ± 0.30	1–3	2.44 ± 0.52	2–3	2.73 ± 0.50	PSI[a]	PSI[a]	FSPGR[a]
Anterior caudate nucleus veins	1–3	2.34 ± 0.81	0–3	1.44 ± 0.74	1–3	2.46 ± 0.57	PSI[a]	FSPGR[b]	FSPGR[a]
Superior choroidal vein	0–1	0.86 ± 0.35	0–2	1.65 ± 0.66	0–2	1.85 ± 0.51	3D CE-MRV[a]	FSPGR[a]	FSPGR[a]
Medial atrial vein	0–3	1.93 ± 0.94	0–3	1.50 ± 0.91	0–3	2.09 ± 1.04	PSI[a]	FSPGR[c]	FSPGR[c]

[a] $P < .001$.
[b] $P < .01$.
[c] $P < .05$.

by using the MinIP technique with 15- to 30-mm thickness in the transverse plane. Reconstructed images were saved once the ICV and tributaries were optimally displayed. A subtraction was performed between the pre- and postcontrast 3D CE-MRV scannings to get images without background pollution. The subtracted images were subsequently reconstructed in the transverse plane by using an MIP algorithm. The MIP images used the same thickness and orientation as the prior PSI-MRV images. 3D CE-FSPGR images were also reformatted with the MIP algorithm in the transverse plane like the 3D CE-MRV images. The same technician performed all image reconstructions.

Image Evaluation

The reconstructed images of PSI-MRV, 3D CE-MRV, and 3D CE-FSPGR were evaluated by a consensus of 2 radiologists with previous experience in PSI and CE-MRV. Source images were reviewed when the radiologists needed to trace or define a vein. Evaluation from another experienced radiologist was obtained when the 2 reviewers failed to agree. The veins evaluated in this study included the ICV, TSV, SV, anterior caudate nucleus vein, superior choroidal vein, and medial atrial vein. Visualization of the veins was qualitatively graded in 4 levels: intense and continuous = 3, faint and continuous = 2, partially visible = 1, invisible = 0. The Wilcoxon signed rank test was

used to analyze differences in the visualization quality of the ICV and its tributaries among the 3 MRV techniques.

Results

The ICV and TSV were clearly and completely displayed at low signal intensity with PSI-MRV in all 80 lateral hemispheres of the 40 patients. They were equally well shown on the 3D CE-MRV and 3D CE-FSPGR images. The SV were delineated best on PSI-MRV, with an average score of 2.9, followed by 3D CE-FSPGR (2.73) and then 3D CE-MRV (2.44) (Table 2 and Fig 1A-C). There were significant differences among the 3 MRV modalities ($P < .001$ for each pair of MRV images). Anterior caudate nucleus veins were shown qualitatively better on PSI-MRV (2.34) than on 3D CE-MRV (1.44) with significant differences ($P < .001$), but inferior to the veins on 3D CE-FSPGR (2.46) ($P < .01$). The superior choroidal vein was poorly delineated in all patients on PSI-MRV, with an average score of 0.86, which was inferior to scores of veins demonstrated on the 3D CE-MRV or 3D CE-FSPGR ($P < .001$ for each pair) (Table 2 and Fig 2A-C). For visualization of the medial atrial vein, PSI-MRV was better than 3D CE-MRV
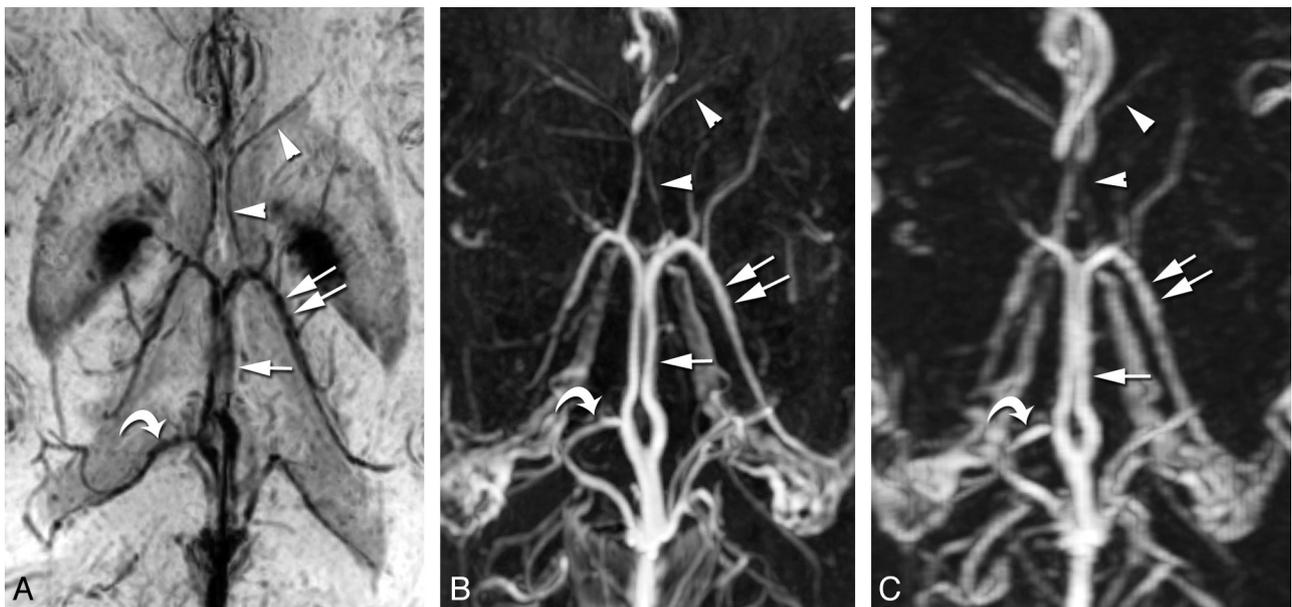
Fig 1. The ICV (*arrow*) and TSV (*double arrows*) are clearly and completely displayed with the PSI-MRV (*A*), 3D CE-FSPGR (*B*), and 3D CE-MRV (*C*) in this patient. The septal veins (*arrowheads*) are delineated best on the PSI-MRV, followed by the 3D CE-FSPGR and then the 3D CE-MRV. The medial atrial vein (*curved arrows*) is easily identified on PSI-MRV, compared with 3D CE-FSPGR and 3D CE-MRV, because of the easy localization of the lateral ventricles and less arterial pollution around the vein of Galen.
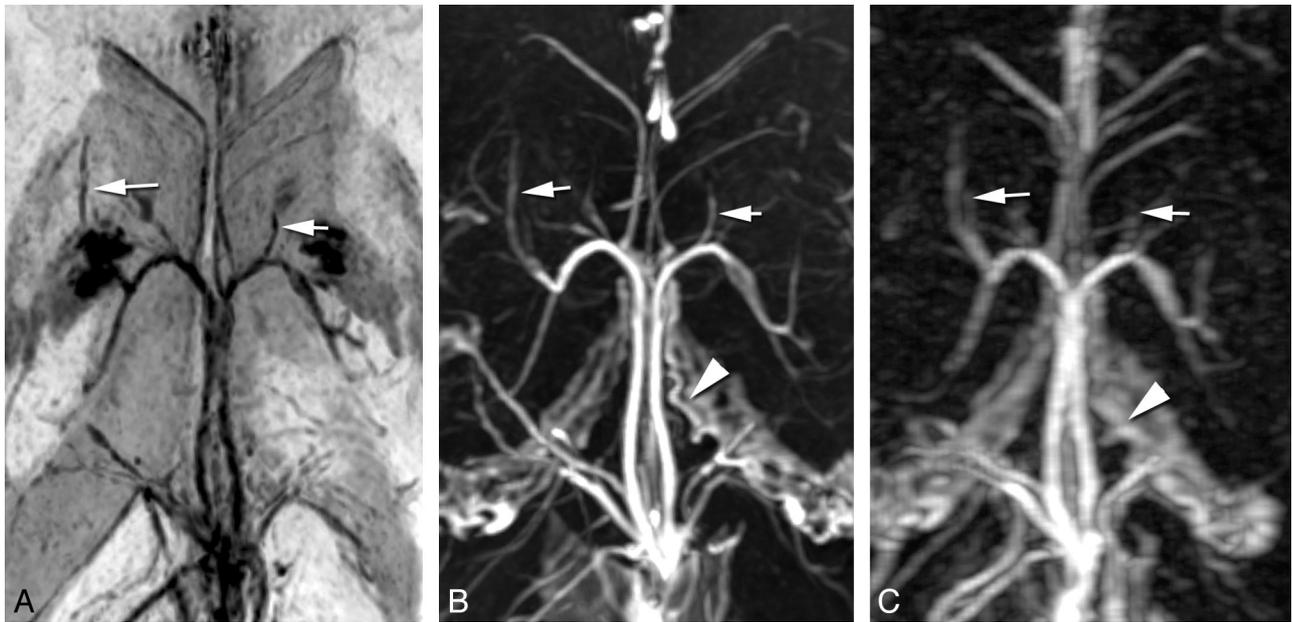
Fig 2. Anterior caudate nucleus veins (*arrow*) are shown qualitatively best on 3D CE-FSPGR (*B*), followed by PSI-MRV (*A*), and then 3D CE-MRV (*C*). The superior choroidal vein (*arrowhead*) is clearly shown on 3D CE-FSPGR (*B*), poorly shown on 3D CE-MRV (*C*), and invisible on PSI-MRV (*A*) in this patient.

($P < .001$) but worse than 3D CE-FSPGR, with a statistical difference ($P < .05$).

Discussion

On the basis of similar principles of SWI, PSI has been introduced to evaluate the variants of ICV noninvasively.[8] With this study, all 3 MRV techniques provided equally good demonstration of the ICV and TSV. The SV were best shown with PSI-MRV among the 3 MRV procedures. The anterior caudate nucleus veins, which comprised several small veins draining inward and backward from the head of the caudate nucleus to the TSV, SV, or ICV, were observed on PSI-MRV with a better image quality than on 3D CE-MRV. The medial atrial vein runs along the medial wall of the atrium and joins the ICV at its terminal portion. With 3D CE-MRV and 3D CE-FSPGR, this vein was commonly confused with other vessels around the vein of Galen. Thus, the reviewers had to carefully identify the vein with the aid of the original image. However, it was quite easy to identify this vein on PSI-MRV because PSI-MRV showed the lateral ventricles clearly and reduced pollution from small arteries around the vein of Galen. The PSI-MRV display of the superior choroidal vein was poor compared with the 3D CE-MRV and 3D CE-FSPGR sequences, possibly because CSF signals obscure the vessel passing the ventricle in PSI MinIP images.

Compared with 3D CE-MRV and 3D CE-FSPGR, using PSI to evaluate deep cerebral veins has several advantages. First, no injection of contrast material is required on PSI-MRV. Second, the PSI-MRV image is free from arterial contamination, which is a big issue on 3D CE-MRV and 3D CE-FSPGR. Finally, the examination can be repeated immediately if the MRV fails for various reasons, because PSI scanning is free of any contamination from brain parenchymal or meningeal contrast enhancement. The examination duration for PSI-MRV is relatively longer than for 3D CE-MRV, but it is almost commensurate with 3D CE-FSPGR. Most patients can tolerate the examination duration.

The basal vein of Rosenthal, another important component of the deep cerebral veins, was not included in this study. A 2-mm-thickness image paralleling the ICV was insufficient to show this vein because it forms an angle to the ICV. An additional acquisition is needed for evaluating the basal vein of Rosenthal. The original image of 3D CE-MRV in this study was designed in the sagittal plane, which enables reliable visualization of the relationship between a meningioma and the superior sagittal sinus. The in-plane spatial resolution of the reconstructed transverse images may underestimate the small tributaries of ICV.

References

1. Giordano M, Wrede KH, Stieglitz LH, et al. **Identification of venous variants in the pineal region with 3D preoperative computed tomography and magnetic resonance imaging navigation: a statistical study of venous anatomy in living patients.** *J Neurosurg* 2007;106:1006–11
2. Kiliç T, Ozduman K, Cavdar S, et al. **The galenic venous system: surgical anatomy and its angiographic and magnetic resonance venographic correlations.** *Eur J Radiol* 2005;56:212–19
3. Kirchhof K, Welzel T, Jansen Q, et al. **More reliable noninvasive visualization of the cerebral veins and dural sinuses: comparison of three MR angiographic techniques.** *Radiology* 2002;224:804–10
4. Lettau M, Sartor K, Heiland S, et al. **3T high-spatial-resolution contrast-enhanced MR angiography of the intracranial venous system with parallel imaging.** *AJNR Am J Neuroradiol* 2009;30:185–87
5. Reichenbach JR, Venkatesan R, Schillinger DJ, et al. **Small vessels in the human brain: MR venography with deoxyhemoglobin as an intrinsic contrast agent.** *Radiology* 1997;204:272–77
6. Reichenbach JR, Jonetz-Mentzel L, Fitzek C, et al. **High-resolution blood oxygen-level dependent MR venography (HRBV): a new technique.** *Neuroradiology* 2001;43:364–69
7. Kurosaki M, Tabuchi S, Akatsuka K, et al. **Application of phase sensitive imaging (PSI) for hemorrhage diagnosis in pituitary adenomas.** *Neurol Res* 2010;32:614–19
8. Fujii S, Kanasaki Y, Matsusue E, et al. **Demonstration of cerebral venous variations in the region of the third ventricle on phase-sensitive imaging.** *AJNR Am J Neuroradiol* 2010;31:55–59